Applied Physics Letters

Experimental reconstruction of the contact resonance shape factor for quantification and amplification of bias-induced strain in atomic force microscopy

Cite as: Appl. Phys. Lett. **114**, 133108 (2019); https://doi.org/10.1063/1.5091803
Submitted: 05 February 2019 . Accepted: 21 March 2019 . Published Online: 05 April 2019

Jason P. Killgore, Akshay Deolia, Lawrence Robins, and Todd W. Murray

Experimental reconstruction of the contact resonance shape factor for quantification and amplification of bias-induced strain in atomic force microscopy

Cite as: Appl. Phys. Lett. **114**, 133108 (2019); doi: 10.1063/1.5091803
Submitted: 5 February 2019 · Accepted: 21 March 2019 ·
Published Online: 5 April 2019

View Online Export Citation CrossMark

Jason P. Killgore,[1,a)] Akshay Deolia,[2] Lawrence Robins,[1] and Todd W. Murray[2]

AFFILIATIONS

[1]Applied Chemicals and Materials Division, National Institute of Standards and Technology, Boulder, Colorado 80305, USA
[2]Department of Mechanical Engineering, University of Colorado, Boulder, Colorado 80309, USA

[a)]**Author to whom correspondence should be addressed:** jason.killgore@nist.gov.

ABSTRACT

The contact resonance (CR) of a surface coupled atomic force microscope (AFM) cantilever can act as an amplifier of AC surface motion for piezoresponse force microscopy and related methods. However, the amplifier properties of the CR vary depending on tip-sample boundary conditions, leading to the appearance of displacement amplitude contrast when only stiffness contrast exists. It was recently proposed that the shape of the vibrating cantilever as a function of CR frequency could be analytically modeled and a shape factor calibration could be applied. Here, we demonstrate an experimental reconstruction of the contact resonance shape factor that can be used to quantify surface displacements in AFM measurements, without reliance on analytical models with uncertain input parameters. We demonstrate accurate quantification of surface displacement in periodically poled lithium niobate and pave the way for quantification of extremely small surface strains in the future.

https://doi.org/10.1063/1.5091803

In piezoresponse force microscopy (PFM) and related techniques such as electrochemical strain microscopy, an alternating current (AC) electric field between a conducting atomic force microscope (AFM) tip and a contacting electromechanically responsive sample will produce a corresponding AC surface strain. By considering the displacement amplitude and the phase of the resultant strain, local variations in the polarization direction, the piezoelectric coefficient, the ion-diffusion, and more can be mapped with nanometer-scale spatial resolution. The properties of devices ranging from random access memory[1] to solar cells[2–4] to energy storage[5] can be inferred from such results. Similarly, AC surface displacements induced by mechanical or thermal excitation of the tip or sample can reveal the mechanical[6,7] and thermal properties[8] of surfaces. AC surface strains are typically measured by detecting the motion of the cantilever with an optical beam deflection system.[9] The beam deflection signal is measured with a quadrant photodetector and sent to a lock-in amplifier to sensitively measure small AC signals. Despite their widespread use in materials science, bias induced strain (BIS) AFM measurements are still subject to numerous artifacts and limitations that can lead to incorrect interpretation of materials response.[10,11] Thus, there is a renewed interest in understanding, eliminating, and/or correcting for the myriad artifacts that can arise during BIS measurements to improve their accuracy and utility.[11–19]

In AC surface strain measurements, the choice of measurement frequency has significant influence on the sensitivity and the accuracy of the results.[13,18,20] Measurement frequencies can be broadly categorized as sub-resonance, off-resonance, and on-resonance with respect to the resonance frequencies of the coupled tip-sample system. Notably, these measurements are performed with the tip in contact with a sample, and thus the contact resonance (CR) properties rather than free resonance properties determine the cantilever dynamics. Quasi-static sub-resonance BIS measurements are the simplest to interpret. This is because the dynamic shape of the vibrating cantilever is identical to the static shape obtained during force vs distance spectroscopy, and hence the dynamic photodetector-voltage to nanometer-displacement conversion s'_{dynamic} is equivalent to the readily calibrated conversion factor s'_{static} (also known as the optical lever sensitivity). To qualify as quasi-static, the measurement must be made far below the 1st CR frequency $f_1^{\,c}$ of the coupled tip-sample system. Off-resonance, but above $f_1^{\,c}$, the cantilever shape is a complex superposition of multiple cantilever eigenmodes determined by the specific forcing acting on the cantilever,[21] making the calculation of s'_{dynamic} difficult. Near f_1^c and at higher frequencies, the vibrational shape of the cantilever is governed by the inertia in the system. The CR vibrational shapes are dependent on the tip-sample boundary conditions, and thus are sensitive to spatial variations in sample modulus, surface topography, tip radius, adhesion, and more.[7,13,16,18,22,23] As a result of this dependence, s'_{dynamic} differs from s'_{static}, and can further vary at every pixel in a BIS AFM image. This can give the appearance of BIS amplitude contrast when only contact stiffness contrast exists. Labuda and Proksch showed that interferometric detection directly at the cantilever tip could reconcile frequency dependent variations in apparent piezoresponse and allow reliable quantification of displacements; however, when sensing displacement directly at the tip, one must directly detect the picometer-scale displacements, without the benefits of resonance amplification.[17] On-resonance, the signal is amplified by the quality factor Q of the CR, which is unitless and typically varies from 10 to 1000, enabling the detection of much smaller displacements than for the sub-resonance case. Overall, a paradox exists where the most sensitive approaches sacrifice accurate quantification, whereas the more accurate approaches sacrifice sensitivity.

In specimens that exhibit large electromechanical strains for a given applied voltage d_{eff} or can accommodate large applied voltages without breakdown, the low-frequency and direct interferometric approaches are attractive. For specimens with much smaller absolute strain response, amplification by the CR provides the only workable detection scheme. CR has been widely used to enhance BIS signals; however, considerations affecting the conversion factor s'_{dynamic}, as discussed above, can quickly lead to erroneous conclusions about the spatial distribution of electromechanical response. Recently, Balke *et al.*[13] proposed the calculation of a unitless CR shape factor λ to convert between the CR amplitude and the absolute cantilever tip displacement u_0. The value of λ is given by

$$\lambda = \frac{A_{peak}}{Q}\frac{1}{u_0 s'_{static}}, \tag{1}$$

where A_{peak} is the peak amplitude in volts of the CR amplitude vs frequency spectrum, measured at the photodetector. The authors used a Euler-Bernoulli (E-B) beam model to calculate λ for a range of values of contact stiffness k_s and cantilever spring constant k_L. It was observed that under particular boundary conditions, λ was nearly independent of k_s, whereas other boundary conditions strongly affected λ. The authors used the calculated λ to quantify CR PFM measurements for a wide range of k_L values, revealing artifacts that can arise due to longer range electrostatic forces. Notably, λ does not depend significantly on Q, but depends on the precise position of the detection laser. Bradler *et al.*[18] extended Balke's approach to incorporate a more comprehensive E-B model. Here, we determine the shape factor experimentally with a calibration artifact whose displacement vs frequency is independently measured by interferometry, and whereby the tip sample contact stiffness can be varied dramatically to cover a broad range of f_1^c and vibrational shapes. The experimental measurement removes inaccuracies that arise due to discrepancies between the E-B model and the real AFM cantilever and the real detection system. A calibrated test cantilever is then used to measure the d_{eff} of periodically poled lithium niobate (PPLN) in CR PFM, showing excellent agreement with previous PFM measurements, but with CR amplification.

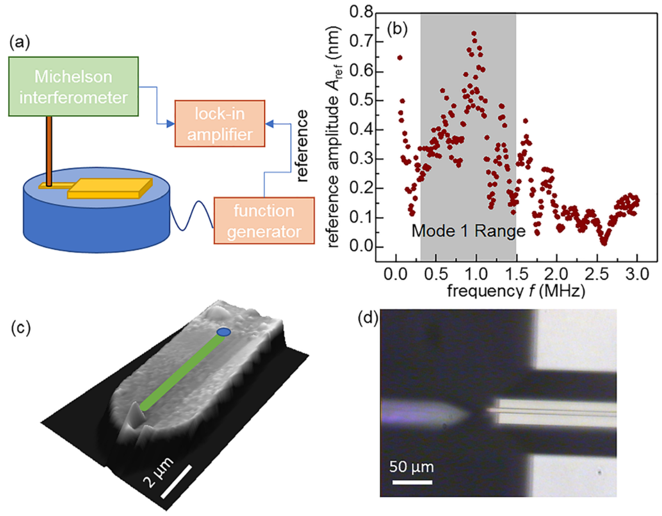

FIG. 1. (a) Schematic of reference artifact calibration. The ultrafast cantilever is attached to the broadband piezo-actuator, then the displacement amplitude vs frequency is determined by driving with a function generator and detecting the interferometer signal with a lock-in amplifier. (b) Reference amplitude vs frequency for the calibration artifact measured at the base of the reference cantilever. The drive amplitude was 2.5 V. (c) Tapping mode AFM scan of the reference cantilever. The green line and the blue circle show the locations of AFM calibration measurements. (d) Optical image of the test (left) and reference (right) cantilevers.

Figure 1 shows the calibration artifact used to measure the shape factor as a function of f_1^c. The artifact is composed of an ultrafast reference cantilever (USC-F2-k3, NanoWorld, Neuchâtel, Switzerland) with a 2.1 MHz fundamental resonance frequency attached to a piezoelectric broadband ultrasound transducer (Accuscan U8401017, Olympus Corporation, Tokyo) with a 2.25 MHz center frequency. The reference cantilever has a length of 10 μm and a width of 5 μm, as confirmed by the tapping mode AFM scan in Fig. 1(c). The ultrasound transducer provides vertical actuation of the reference cantilever. The displacement of the reference cantilever was measured with a Michelson laser interferometer (Sonus, Rudolph Technologies, Wilmington, MA) focused at the cantilever's base. A function generator provided a 2.5 V (all voltages are zero-to-peak) drive signal to the actuator at frequencies f from 50 kHz to 3 MHz.

The surface displacement ampltiude $A_{\text{ref}}(f)$ of the reference cantilever was calculated from

$$A_{ref}(f) \approx \frac{\psi V_{HF}(f)}{2\pi V_{LF}}, \tag{2}$$

where ψ is the wavelength of the laser, $V_{\text{HF}}(f)$ is the high-frequency time-varying voltage signal from the photodetector as observed at the lock-in amplifier, and V_{LF} is the voltage of the low-frequency output of the photodetector ($V_{\text{LF}} = 3.75$ V).[24]

The A_{ref} vs f response of the reference cantilever, measured near the cantilever base, is shown in Fig. 1(b). Over the full frequency range, the mean value of A_{ref} is 245 pm $\pm$ 156 pm. The frequency-varying response of A_{ref} is typical of the broadband fingertip-type ultrasound actuator, which is heavily damped over the few megahertz frequency range. When measurements were repeated closer towards the cantilever's free end, a clear peak at 2.17 MHz corresponding to the fundamental resonance of the reference cantilever was apparent. The high fundamental resonance frequency enables the reference cantilever to be approximated as a quasistatic device when subsequently calibrating a test cantilever in the 100 kHz to 1 MHz frequency range typical of PFM measurements. The range of CR frequencies for our test cantilever (ElectriTap 300G, BudgetSensors, Sofia, Bulgaria), which exhibits $k_L = 28$ N/m and the first free resonance frequency $f_1^\circ = 246$ kHz, is highlighted in gray. Notably, the interferometer measures surface displacement A_{ref}, whereas Eq. (1) requires the tip displacement u_0. The value of A_{ref} can be translated into u_0 by $u_0 = A_{ref} - \delta$, where δ is the dynamic tip-sample indentation. In a CR measurement, δ is not easily calculated, and for the purpose of calculating materials properties such as piezoelectric coefficient, it is more desirable to measure the dynamic surface strain in the absence of any indentation. Thus, we amend Eq. (1) to

$$\lambda' = \frac{A_{peak}}{Q}\frac{1}{A_{ref}\, s'_{static}}, \tag{3}$$

where λ' is the surface displacement shape factor rather than the tip displacement shape factor.

As we have demonstrated previously on a microbridge sample,[21,22,25] suspended microstructures provide ideal test structures for widely and intentionally varying f_1^c. On suspended structures, the effective contact stiffness depends on the series sum of the bending stiffness of the structure and the contact stiffness of the interacting materials. The bending stiffness varies cubically with the distance along the reference structure, and thus can be chosen based on the contact position of the test cantilever. Here, we used a single cantilever instead of a double cantilevered microbridge because of the commercial availability of such high resonance-frequency devices for high-speed AFM.[26] As shown in Fig. 1(d), a test cantilever is brought close to the smaller reference cantilever, then an image of the reference cantilever is produced by scanning with the test cantilever. The reference cantilever image enables subsequent positioning of the test cantilever tip at various locations on the reference cantilever. Figure 2(a) shows a series of amplitude vs frequency spectra obtained at a constant applied force for different positions of the test cantilever tip along the reference cantilever (green spectra) and for different applied forces at a particular location on the support chip (blue spectra). The locations for the spectra are indicated by green and blue markings in Fig. 1(c). Position dependent spectra were acquired 9.1 nm apart along the long axis of the reference cantilever. Force dependent spectra were acquired in 65 nN steps from 0 to 6.5 μN. The detection laser was located near the end of the test cantilever [shown in the inset to Fig. 2(a)], resulting in $s'_{static} = 0.021$ V/nm. The reference cantilever actuator was driven with a voltage of 0.05 V, resulting in sufficiently small amplitude to ensure that the tip-sample interaction remained linear, as indicated by the symmetric shape of the resonance peaks.[27] Moving the contact point for the test cantilever away from the base of the reference cantilever towards the free end results in a reduction of f_1^c. Conversely, increasing the applied force for contact with the support chip allows higher f_1^c to be obtained. From Fig. 2(a), a substantial variation in A_{peak} vs f is obtained over different boundary conditions. Notably, the frequency dependence of A_{peak} is not a 1:1 reflection of the calibrated response in Fig. 1(b). Figure 2(b) shows plots of A_{peak} and Q determined from a damped harmonic oscillator (DHO) fit as a function of f_1^c. Some of the variation in A_{peak} vs f_1^c is mirrored in the Q vs f_1^c plot. The non-constant value of the resultant A_{peak}/Q signal plotted in Fig. 2(c)

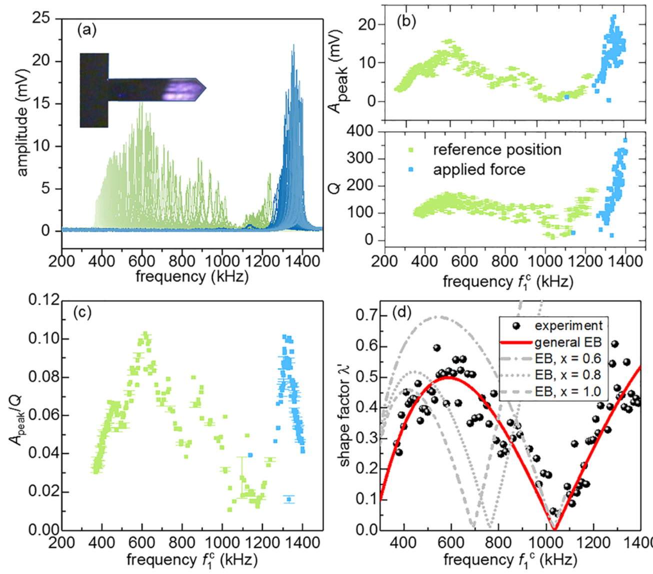

FIG. 2. (a) Contact resonance spectra acquired with a test cantilever in contact with a reference cantilever at different locations (green) and forces (blue). Inset shows the detection laser position on the test cantilever. (b) Variation in the peak amplitude and the quality factor of the CR spectra shown in (a) as a function of CR frequency. (c) Peak amplitude divided by the quality factor. Some of the structure observed in Fig. 1(b) is reproduced in Fig. 2(c); the remaining difference is attributed to the shape factor. (d) Contact resonance shape factor experimentally determined by equating the reference displacement in Fig. 1(b) to the drive amplitude A_{peak}/Q measured in Fig. 2(c). The fit is a least squares regression to the derivative of the general spatial solution for a Euler-Bernoulli beam under arbitrary boundary conditions. Simulations are also shown for an E-B model under simple spring boundary conditions and with a variable detection position.

provides direct evidence of the influence of λ' on the observed amplitude. Based on the linear relation between the reference amplitude and the drive amplitude observed in the interferometric calibration, the value of A_{ref} was scaled by the ratio of drive amplitudes to the actuator in AFM calibration and interferometer calibration steps. Data for A_{ref} and A_{peak}/Q were resampled by linear interpolation to 10 kHz spacing, then Eq. (3) was used to directly calculate the frequency dependence of the shape factor λ', as shown in Fig. 2(d). The shape factor varies from 0 to $\approx$0.6 with changing f_1^c. The minimum in λ' at $f_1^c \approx 1$ MHz corresponds to a vibrational antinode of the cantilever; at an antinode, there is negligible response amplitude from the cantilever regardless of the drive amplitude. Notably, the slope $d\lambda'/df_1^c$ is large everywhere outside a narrow frequency range from 500 kHz to 750 kHz, suggesting that ascribing variations in A_{peak}/Q to variations in surface strain without considering the corresponding λ' could have highly misleading consequences. To put the experimentally determined shape factor into a more useful form for PFM measurement, the experimental data were fit to the absolute value of the derivative of the general spatial solution for the first eigenmode $j(x)$ given by the Euler-Bernoulli beam model

$$j(x) = \left| \frac{\partial}{\partial x}\begin{pmatrix} A_1(\mathrm{Cos}\,\beta x + \mathrm{Cosh}\,\beta x) + A_2(\mathrm{Cos}\,\beta x - \mathrm{Cosh}\,\beta x) \\ + \cdots A_3(\mathrm{Sin}\,\beta x + \mathrm{Sinh}\,\beta x) + A_4(\mathrm{Sin}\,\beta x - \mathrm{Sinh}\,\beta x) \end{pmatrix} \right|. \tag{4}$$

In Eq. (4), A1, A2, A3, and A4 are adjustable fit parameters, x is the fractional position along the cantilever, and β is a reduced wavenumber given by $\beta = 1.875(f_1^c/f_1^0)^{0.5}$.

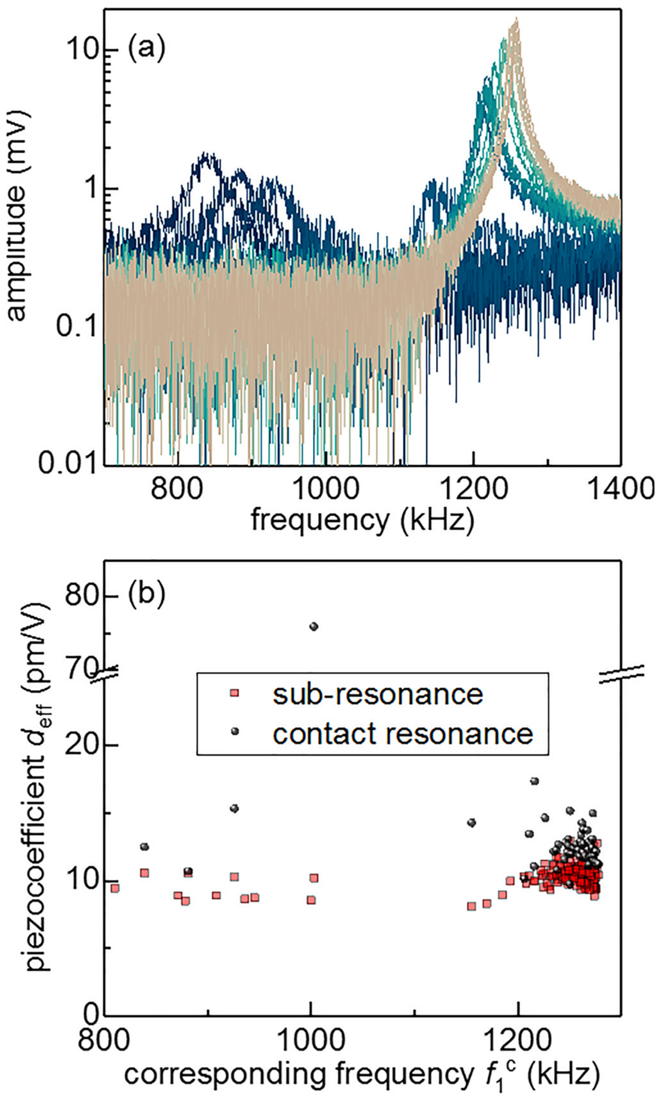

FIG. 3. (a) Piezoresponse force microscopy data acquired on a periodically poled lithium niobate sample at 1 V drive amplitude. Force was varied from 0 to 6.1 μN in 210 nN steps to produce the variation in contact resonance frequency. (b) The effective piezo-coefficient for PPLN determined from the measurements in (a) combined with the shape factor results in Fig. 2(c). The outlier around $f_1^c \approx 1$ MHz is due to the near-zero shape factor at that frequency. Also shown are sub-resonance PFM data acquired simultaneously with the CR PFM data.

As shown in Fig. 2(d), the model provides an excellent fit to the experimental data. Figure 2(d) also presents plots of λ' vs f_1^c from the simplest possible E-B model used in CR-FM analysis. Here, the tip-sample contact is modeled as a single spring located at the end of the cantilever. Three different values of x are plotted, showing dramatic variation in λ' vs f_1^c even for this simplest model. Increasingly complex models considering the tip offset, the lateral stiffness, and the cantilever tilt still exhibited large degrees of variability with relatively small changes to input parameters and did not agree better with the experimental result than the general fit to Eq. (4). Thus, for absolute quantification of the shape factor, the experimental calibration provides distinct advantages.

To demonstrate the validity of our approach for the experimental reconstruction of the shape factor, the reference cantilever was replaced by a PPLN sample without altering the position of the detection laser on the test cantilever. The test cantilever was brought into contact with the PPLN and an AC bias voltage of 1.0 V was applied between the tip and the sample. Amplitude vs frequency spectra were acquired while the applied force was varied from 0 to 6.1 μN in 210 nN steps to produce a range of contact stiffness, and thus f_1^c values [Fig. 3(a)], similar to the contact stiffness variation that is known to occur on mechanically or topographically heterogeneous samples while imaging. Similar to the calibration dataset, the amplitude and the quality factor are seen to vary significantly over the observed range of f_1^c. Fitting the results to the DHO model and using λ' from the fit in Fig. 2(d) allow for absolute quantification of d_{eff} as shown in Fig. 3(b). Ignoring the lone outlier that resulted from an antinode at $f_1^c \approx 1$ MHz, we measure a value of $d_{eff} = (12.2 \pm 1.3)$ pm/V. Figure 3(b) also shows traditional sub-resonance PFM measurements acquired from an average of the cantilever response between 5 kHz and 10 kHz, and calibrated with s'_{static}. The data were acquired simultaneously with the CR results, and thus each low-frequency measurement corresponds with an applied force and a value of f_1^c. Data are shown for 1 V, 3 V, and 5 V AC drive amplitudes. The sub-resonance $d_{eff} = (10.1 \pm 0.9)$ pm/V is ≈16% lower than the CR PFM result. The small but systematic discrepancy may be attributable to the inherent subtraction of indentation in the CR PFM result and uncertainties in the measurement of s'_{static} and V_{LF}. Like in previous PFM measurements, the resultant d_{eff} is lower than the bulk-measured values, likely due to inhomogeneity in the electric field.[28] We note that the calibrated CR PFM result achieves similar mean and standard deviation values as the sub-resonance result, but benefits from up to 400× amplification via Q, enabling correspondingly smaller signals to be quantified. The optimization of piezoresponse detection coincides with the maximum in A_{peak}, which occurs when the product $Q\lambda'$ is maximized.

Overall, the experimental measurement of the shape factor is an effective means to achieve quantitative measurement of extremely small surface displacements. The approach eliminates one of the critical tradeoffs between on-resonance and sub-resonance PFM methods, allowing both high sensitivity and high accuracy.

REFERENCES

[1]P. Sharma, Q. Zhang, D. Sando, C. H. Lei, Y. Liu, J. Li, V. Nagarajan, and J. Seidel, Sci. Adv. 3(6), e1700512 (2017).

[2]I. M. Hermes, S. A. Bretschneider, V. W. Bergmann, D. Li, A. Klasen, J. Mars, W. Tremel, F. Laquai, H.-J. Butt, M. Mezger, R. Berger, B. J. Rodriguez, and S. A. L. Weber, J. Phys. Chem. C **120**(10), 5724–5731 (2016).

[3]Y. Liu, L. Collins, R. Proksch, S. Kim, B. R. Watson, B. Doughty, T. R. Calhoun, M. Ahmadi, A. V. Ievlev, S. Jesse, S. T. Retterer, A. Belianinov, K. Xiao, J. Huang, B. G. Sumpter, S. V. Kalinin, B. Hu, and O. S. Ovchinnikova, Nat. Mater. **17**, 1013–1019 (2018).

[4]G. A. MacDonald, C. M. Heveran, M. Yang, D. Moore, K. Zhu, V. L. Ferguson, J. P. Killgore, and F. W. DelRio, ACS Appl. Mater. Interfaces **9**(39), 33565–33570 (2017).

[5]N. Balke, S. Jesse, Y. Kim, L. Adamczyk, A. Tselev, I. N. Ivanov, N. J. Dudney, and S. V. Kalinin, Nano Lett. **10**(9), 3420–3425 (2010).

[6]J. P. Killgore and F. W. DelRio, Macromolecules **51**(18), 6977–6996 (2018).

[7] U. Rabe, in *Applied Scanning Probe Methods II: Scanning Probe Microscopy Techniques*, edited by B. Bhushan and H. Fuchs (Springer, Berlin Heidelberg, 2006), pp. 37–90.
[8] J. Varesi and A. Majumdar, Appl. Phys. Lett. **72**(1), 37–39 (1998).
[9] G. Meyer and N. M. Amer, Appl. Phys. Lett. **56**(21), 2100–2101 (1990).
[10] R. K. Vasudevan, N. Balke, P. Maksymovych, S. Jesse, and S. V. Kalinin, Appl. Phys. Rev. **4**(2), 021302 (2017).
[11] D. Seol, B. Kim, and Y. Kim, Curr. Appl. Phys. **17**(5), 661–674 (2017).
[12] N. Balke, S. Jesse, Y. Kim, L. Adamczyk, I. N. Ivanov, N. J. Dudney, and S. V. Kalinin, ACS Nano **4**(12), 7349–7357 (2010).
[13] N. Balke, S. Jesse, P. Yu, B. Carmichael, S. V. Kalinin, and A. Tselev, Nanotechnology **27**(42), 425707 (2016).
[14] N. Balke, S. Jesse, B. Carmichael, M. B. Okatan, I. I. Kravchenko, S. V. Kalinin, and A. Tselev, Nanotechnology **28**(6), 065704 (2017).
[15] S. Kim, D. Seol, X. Lu, M. Alexe, and Y. Kim, Sci. Rep. **7**, 41657 (2017).
[16] R. Proksch, J. Appl. Phys. **118**(7), 072011 (2015).
[17] A. Labuda and R. Proksch, Appl. Phys. Lett. **106**(25), 253103 (2015).
[18] S. Bradler, A. Schirmeisen, and B. Roling, J. Appl. Phys. **122**(6), 065106 (2017).
[19] G. A. MacDonald, F. W. DelRio, and J. P. Killgore, Nano Futures **2**(1), 015005 (2018).
[20] S. Jesse, B. Mirman, and S. V. Kalinin, Appl. Phys. Lett. **89**(2), 022906 (2006).
[21] R. Wagner and J. Killgore, Nanotechnology **28**(10), 104002 (2017).
[22] R. Wagner, J. P. Killgore, R. C. Tung, A. Raman, and D. C. Hurley, Nanotechnology **26**(4), 045701 (2015).
[23] R. Wagner, A. Raman, and R. Proksch, Appl. Phys. Lett. **103**(26), 263102 (2013).
[24] D. C. Hurley and C. M. Fortunko, Meas. Sci. Technol. **8**(6), 634 (1997).
[25] R. Wagner and J. P. Killgore, Appl. Phys. Lett. **107**(20), 203111 (2015).
[26] T. Ando, Biophys. Rev. **10**(2), 285–292 (2018).
[27] D. Rupp, U. Rabe, S. Hirsekorn, and W. Arnold, J. Phys. D: Appl. Phys. **40**(22), 7136 (2007).
[28] T. Jungk, Á. Hoffmann, and E. Soergel, Appl. Phys. A **86**(3), 353–355 (2007).